2013 IEEE/RSJ International Conference on
Intelligent Robots and Systems (IROS)
November 3-7, 2013. Tokyo, Japan

Cartesian Stiffness Evaluation of a Novel 2 DoF Parallel Wrist under Redundant and Antagonistic Actuation†

Cheng Li[1], Yuanqing Wu[1], Jiachun Wu[1], Weiyi Shi[1], Dan Dai[1], Jinbo Shi[1] and Zexiang Li[1]

***Abstract*— In this paper, we present an experimental evaluation of the Cartesian stiffness of a novel parallel wrist under redundant and antagonistic actuation. The mechanism in consideration is Omni-Wrist V (*OW*5), a two degrees-of-freedom (DoF) parallel mechanism redundantly actuated by three subchains. We first give a brief review of its kinetostatics and derive its reduced Cartesian stiffness model. To illustrate the stiffness enhancement of *OW*5 under redundant and antagonistic actuation, its Cartesian stiffness is measured and evaluated under four control schemes: the non-redundant control, the minimum 2-norm torque control without or with redundant encoder, and the antagonistic actuation control. Measurement data are represented using stiffness matrices and stiffness ellipses. Our study offers a quick quantitative evaluation of stiffness enhancement of *OW*5 under redundant and antagonistic actuation.**

I. INTRODUCTION

A. Redundant and antagonistic actuation of parallel mechanisms

Recently, there is an interesting trend towards the use of parallel robots for applications with higher demands on accuracy and stiffness, etc [1]. In order to achieve high stiffness for such applications as cutting and milling, the robot should have both an appropriate geometry and a simple yet efficient stiffness control paradigm. Although there is an ongoing debate over whether serial or parallel mechanisms should be chosen for machining robot development [2], growing evidence shows that a properly designed parallel mechanisms can achieve high stiffness, accuracy and payload without the costly linear bearings [3]–[5]. Moreover, the existence of kinematic loops in a parallel mechanism allows for redundant actuation that further increases its stiffness and payload [6]–[9].

In particular, antagonistic actuation creates an effective stiffness directly analogous to that of a wound metal spring [7]; the effective stiffness is therefore referred to as antagonistic stiffness [10]–[12]. The antagonistic stiffness is related to both the second order geometry of the mechanism and redundant input torques [10]. Alternatively, the redundant input torques may be used to reduce average or maximum input torques [8], increase end-effector force capability [13], or eliminate backlash [14]. Almost all the aforementioned work use only simulations to test their control or force optimization algorithm. The types of parallel mechanisms considered are almost exclusively planar [12], [14], [15]. Few experiment results on practical spatial parallel mechanisms can be found in the literature.

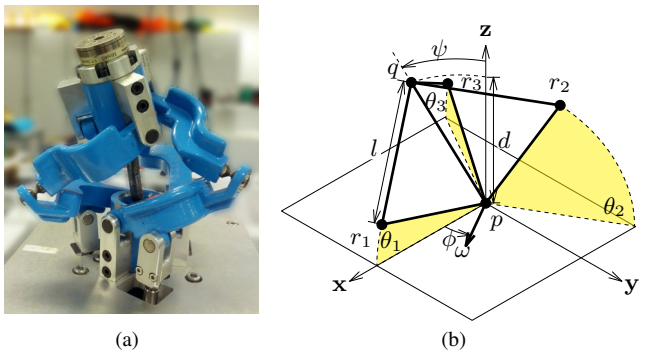

(a) (b)

Fig. 1. (a) Ross Hime's Omni-Wrist V [16]; (b) Simplified geometry of Omni-Wrist V.

In this paper, we consider the redundant actuation of Omni-Wrist V (*OW*5) [16], a spatial parallel mechanism with two rotational DoF (see Fig. 1(a)). Our study is for the proof-of-concept of *OW*5 as a rotary module providing extra rotational DoF for three-axes milling machine and SCARA assembly line. To the authors' knowledge, it is also the first attempt to apply redundant actuation to a real spatial parallel mechanism.

B. Omni-Wrist V: the new parallel wrist

Ross Hime's Omni-Wrist V is invented by Mark Rosheim in an effort to mimic the human shoulder movement in terms of both its parallel nature and its extraordinary rotation range [16] . As shown in Fig. 1, the mechanism has a passive double ball bar (or a $\mathcal{SS}$ subchain), and three actuating revolute-spherical-revolute (denoted $\mathcal{RSR}$) subchains axially symmetric about the passive $\mathcal{SS}$ subchain. Its unique kinematics offers an extraordinary rotation range of 90° about a pencil of revolute axes. The unique kinematics that underlies the high rotation range of Omni-Wrist III (slightly different from but equivalent to *OW*5) is extensively studied in our previous work [17], [18]. With some preliminary experiments, *OW*5 exhibits the promised rotation range, but has a relatively poor stiffness due to clearance in the spherical joints and force asymmetry when only two $\mathcal{RSR}$ subchains are actuated. This together with the fact that *OW*5 can naturally be redundantly actuated makes *OW*5 an ideal testbed for redundant actuation control algorithms.

†This project is supported by RGC Grant No.616509, No.615610 and No.615212, and by National Basic Research Program of China (973 Program, Grant No.2011CB013104), and by Key Joint Project of National Natural Science Foundation of China (Grant No.U1134004), Shenzhen Municipal Science and Technology Planning Program for Basic Research No. JCYJ20120618150931822

[1]Department of Electronic and Computer Engineering, Hong Kong University of Science and Technology, Clear Water Bay, Kowloon, Hong Kong {cliac,eetroywu,jwuae,wshi,ddai,bozishi,eezxli}@ust.hk

C. Stiffness modeling and analysis of parallel mechanisms

Mathematically, Cartesian stiffness is the Hessian of the mechanism's elastic potential. When computed with a set of generalized end-effector coordinates, the stiffness matrix is symmetric [19]–[21]. Practically, it is more reasonable to directly compute the ratio between end-effector wrench and twist displacements, which in general results in asymmetric stiffness matrices [22], [23]. In our current study, we use an ATI force-torque sensor to directly measure the external load wrench, and a camera to measure the end-effector twist displacement. Therefore, we shall adopt the second definition in this paper.

Numerous studies on stiffness modeling and analysis of parallel mechanisms have been conducted in the literature. The main challenge is always finding a tradeoff between accuracy and ease of computation. The virtual joint approach proposed by [19] and [20] considered only joint stiffness in an attempt to derive an analytical or parametric model for optimization. Reference [24] and [25] used matrix structural analysis to provide a more accurate analytical stiffness model. A good summary and improvement can be found in [26]. A suitable analytical stiffness model for *OW*5 will be derived in future study and verified using the experiment data acquired in the current study.

D. Organization of the paper

This paper is organized as follows: in Section II, we first give a brief review of the kinetostatics of *OW*5 using the standard tool of screw theory and homogenous matrix [27]. We show that its kinetostatics reduces to that of a point on a sphere. Moreover, a preferred basis for the actuation and constraint wrenches can be chosen. The stiffness model of *OW*5 also reduces to two dimensional twist and wrench subspaces. In Section III, we propose four control strategies for stiffness evaluation of *OW*5: joint space PID control, minimum 2-norm torque control without or with redundant encoder, and the antagonistic actuation control. We present the experiment setup and results in Section IV and draw our conclusion in Section V.

II. Kinetostatic Analysis of Omni-Wrist V

The conceptual design of *OW*5 is closely related to the well known constant velocity (CV) couplings [28]. The geometry and kinetostatics of *OW*5 can be easily explained using screw theory [28], [29]. Our earlier work provides a finite motion analysis for *OW*5 [17], [18].

A. Mechanism description and kinematics

The geometry of *OW*5 can be summarized as follows (see also Fig. 1(b)):

1) At initial configuration, the three $\mathcal{RSR}$ subchains are axial symmetric about the double ball bar pq (with length d), i.e. 120° away from each other.
2) At any configuration, the locations of the three $\mathcal{S}$ joints from the three $\mathcal{RSR}$ subchains (denoted by r_1, r_2 and r_3) define a plane about which the whole mechanism is completely mirror symmetric.
3) The three actuated $\mathcal{R}$ joints (variables denoted by θ_i) are located on the base side of plane $r_1r_2r_3$. Their axes are coplanar, and intersect at p. Similarly, the three passive $\mathcal{R}$ joints are coplanar and intersect at q.
4) By mirror symmetry, pq is always perpendicular to the plane $r_1r_2r_3$. $\|qr_i\| = \|pr_i\| = l, i = 1, 2, 3$.
5) Fix a base frame as shown in Fig. 1(b). $\mathbf{z}$-axis is aligned with the initial configuration of pq; the $\mathbf{x}$-axis is chosen so that pr_1 lies in the $\mathbf{xz}$ plane. Fix a body frame to the end-effector such that it coincides with the base frame at the initial configuration (so that there will be no initial coordinate transformation).
6) the end-effector motion of *OW*5 is completely determined by the current location of q: if pq rotates away from the $\mathbf{z}$-axis by axis ω and angle ψ, the rotation matrix of the end-effector is given by $e^{2\hat{\omega}\psi}$. *OW*5's *end-effector space* E is therefore given by:

$$E = \left\{ g = \begin{bmatrix} e^{2\hat{\omega}\psi} & d(e^{\hat{\omega}\psi} - e^{2\hat{\omega}\psi})\mathbf{z} \\ 0 & 1 \end{bmatrix} \middle| \omega = \mathbf{x}c_\phi + \mathbf{y}s_\phi \right\} \quad (1)$$

where c_ϕ, s_ϕ stand for $cos(\phi)$ and $sin(\phi)$ respectively. E is a two dimensional submanifold of the special Euclidean group $SE(3)$, which can either be parameterized by the spherical coordinates of q:

$$q = g \cdot d\mathbf{z} = de^{\hat{\omega}\psi}\mathbf{z} = (ds_\psi s_\phi, -ds_\psi c_\phi, dc_\psi) \quad (2)$$

or by two of the three actuation variables, say $\theta_e = (\theta_1, \theta_2)$. The effective actuation variables θ_e also uniquely parameterizes the redundant actuation variables $\theta_a = (\theta_1, \theta_2, \theta_3)$. The relation between various parametrizations is clear from Fig. 2, where $\Theta_e = \{\theta_e\}$ is the *effective joint space*, $\Theta_a =$

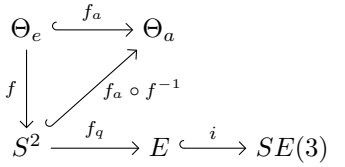

Fig. 2. Parametrization diagram of the pose space E

$\{\theta_a\}$ denotes the *redundant joint space*, and S^2 denotes the two dimensional sphere with radius d. The spherical parametrization $f_q : q \mapsto g$ can be computed from (2); the forward kinematics map $f : \theta_e \mapsto q$ and inverse kinematics map $f_a \circ f^{-1} : q \mapsto \theta_a$ can be found in [18].

B. Kinetostatic analysis of *OW*5

By taking differentiation of the parametrization diagram in Fig. 2 at a general configuration, we acquire a diagram of tangent spaces and Jacobians as shown in Fig. 3. Here, T_qS^2 is the tangent plane of the sphere at q, and T_gE is the twist subspace of the twist space $se(3)$ at g. Usually, the inverse jacobian $J_I = J_a \circ J^{-1}$ is easier to evaluate and often used in the literature [10]. It is straightforward to verify that $T_gE = span\{\xi_1, \xi_2\}$ with:

$$\xi_1 = (-e^{\hat{\omega}\psi}\mathbf{x} \times \frac{q}{2}, e^{\hat{\omega}\psi}\mathbf{x})^T, \xi_2 = (-e^{\hat{\omega}\psi}\mathbf{y} \times \frac{q}{2}, e^{\hat{\omega}\psi}\mathbf{y})^T \quad (3)$$

ξ_1 and ξ_2 are in fact zero-pitch twists passing through the midpoint of pq and also lying in the mirror plane (the yellow plane in Fig. 4) [17], [18].

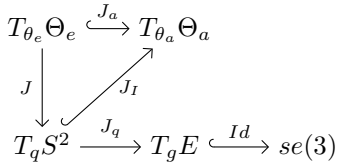

Fig. 3. Tangent diagram of Fig. 2

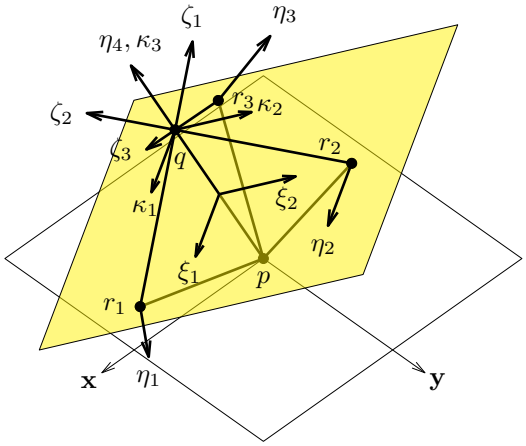

Fig. 4. Twist and Wrench system of Omni-Wrist V: admissible twists: ξ_1, ξ_2; constraint wrenches: $\eta_1, \eta_2, \eta_3, \eta_4$; actuation wrenches: $\zeta_1, \zeta_2, \zeta_3$.

The tangent diagram in Fig. 3 admits a dual or cotangent diagram as shown in Fig. 5. In the dualization process, the Jacobian maps are replaced by their pull-backs and injective maps are replaced by surjective maps. The dual spaces $T^*_{\theta_e}\Theta_e$ and $T^*_{\theta_a}\Theta_a$ denote the spaces of effective and redundant torque vectors respectively; T^*_gE is the subspace of actuating wrenches in the wrench space $se(3)^*$. Using the natural pair $\langle , \rangle$ between twists and wrenches, the constraint wrench space $T^*_gE^\perp$ is given by:

$$T^*_gE^\perp = \{\eta \in se(3)^* | \langle \eta, \xi \rangle = 0, \forall \xi \in T_gE\} \quad (4)$$

The following equation shows that $T^*_gE^\perp = \ker Id^T$:

$$\langle \eta, \xi \rangle = \langle \eta, Id(\xi) \rangle = \langle Id^T(\eta), \xi \rangle = 0, \forall \xi \in T_gE \quad (5)$$

It is clear that $se(3)^* = T^*_gE \oplus T^*_gE^\perp$. However, there is no natural choice of inner product for $se(3)$ or $se(3)^*$ and T^*_gE is by no means the orthogonal complement of $T^*_gE^\perp$. In fact, T^*_gE as a subspace of $se(3)^*$ is not uniquely defined. Nevertheless, it is convenient to assign some special bases for both wrench subspaces using observation method [30], which we show in Fig. 4.

Now, we shall use Fig. 5 to give a simple description of the redundant actuation problem. A torque vector $\tau_a \in T^*_{f_a(\theta_e)}\Theta_a$ is said to be an *internal torque* if it exerts no output force. Therefore the subspace of internal torques is nothing but $\ker J_I^T$. The following orthogonal decomposition is at the heart of all redundant actuation control schemes:

$$T^*_{f_a(\theta_e)}\Theta_a = \ker J_I^T \oplus Im(J_I^+), J_I^+ = J_I(J_I^T J_I)^{-1} \quad (6)$$

Since J is an isomorphism, the above equation is the same as:

$$T^*_{f_a(\theta_e)}\Theta_a = \ker J_a^T \oplus Im(J_a^+), J_a^+ = J_a(J_a^T J_a)^{-1} \quad (7)$$

When τ_a is set to $J_a^+\tau_e$, we have the minimum 2-norm torque control [8]. Alternatively, τ_a is set to $J_a^+\tau_e + A\lambda$ where the column vectors of A span $\ker J_a^T$ and λ is chosen to be a constant component vector [12]. The internal torque can be further scheduled to be a function of the mechanism's states.

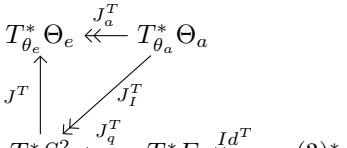

Fig. 5. Cotangent diagram of Fig. 2

C. Reduced kinetostatics and stiffness model of *OW*5

We have shown that the kinetostatics of *OW*5 is virtually that of q on the sphere (although the inertial distribution is different from that of a point mass). This generates the following commutative diagrams:

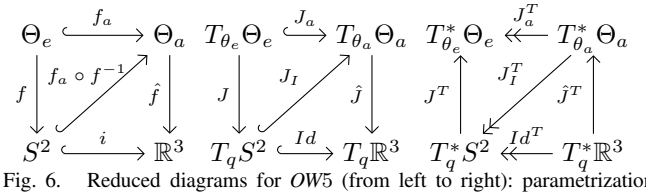

Fig. 6. Reduced diagrams for *OW*5 (from left to right): parametrization diagram; tangent diagram; cotangent diagram.

where i is the embedding of S^2 in $\mathbb{R}^3$. $\hat{f}$ is the forward kinematics map of *OW*5 with double ball bar removed, or a Canterbury wrist [31]. The wrench space reduces to $T^*_q\mathbb{R}^3$, the bundle of pure force at q which is spanned by ζ_1, ζ_2 and ζ_3. In this case, $T^*_gE^\perp$ is the one dimensional subspaces of pure forces normal to T_qS^2. Since $T^*_q\mathbb{R}^3$ has a natural inner product, the orthogonality between T^*_gE and $T^*_gE^\perp$ can be defined. If we choose the following bases for $T^*_q\mathbb{R}^3$ (see Fig. 4):

$$\begin{cases} \kappa_1 = (e^{\hat{\omega}\psi}\mathbf{x}, -e^{\hat{\omega}\psi}\mathbf{x} \times q)^T \\ \kappa_2 = (e^{\hat{\omega}\psi}\mathbf{y}, -e^{\hat{\omega}\psi}\mathbf{y} \times q)^T \\ \kappa_3 = (e^{\hat{\omega}\psi}\mathbf{z}, -e^{\hat{\omega}\psi}\mathbf{z} \times q)^T \end{cases} \quad (8)$$

we have $T^*_gE = span\{\kappa_1, \kappa_2\}$ and $T^*_gE^\perp = span\{\kappa_3\}$. Moreover, we have $\ker J_I^T = \hat{J}^T(T^*_gE^\perp)$. Note that $T^*_gE^\perp$ has a different physical meaning in the reduced model. It corresponds exactly to the internal torques via the isomorphism $\hat{J}^T$. In this case, we refer to $T^*_gE^\perp = span\{\kappa_3\}$ as the *internal force space*.

Cartesian stiffness linearly relates external wrench F applied at the end-effector with corresponding twist displacement $\Delta g \cdot g^{-1}$, and is therefore characterized by a 6-by-6 matrix $\mathcal{K}$:

$$\mathcal{K} : se(3) \to se(3)^*, \Delta g \cdot g^{-1} \mapsto F = \mathcal{K}(\Delta g \cdot g^{-1}) \quad (9)$$

Under the reduced kinetostatics model, we have a reduced 2-by-2 stiffness matrix $\mathcal{K}_r$:

$$\mathcal{K}_r : T_gE \to T^*_gE, \alpha_1\xi_1 + \alpha_2\xi_2 \mapsto \beta_1\kappa_1 + \beta_2\kappa_2 \quad (10)$$

using the bases ξ_1, ξ_2 and κ_1, κ_2. According to Section I, $\mathcal{K}_r$ is in general asymmetric. Although $\mathcal{K}_r$ does not account for all stiffness information of the wrist, it is enough for the evaluation of stiffness enhancement by redundant and antagonistic actuation. The complete Cartesian stiffness $\mathcal{K}$ is the subject to our future study.

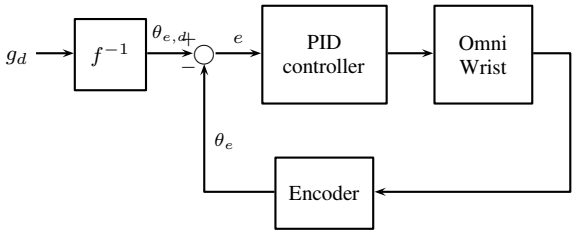

Fig. 7. Joint space PID control scheme

III. Control Schemes

In this section, three different control strategies are formulated for *OW*5.

A. Joint space PID control

In this control scheme, only the effective joint variables $\theta_e = (\theta_1, \theta_2)^T$ are actuated and controlled independently using PID controllers (see Fig. 7).

B. Minimum 2-norm torque control

All three motors are used to actuate *OW*5 in this control scheme to achieve a minimum 2-norm redundant torque vector τ_a. Since a constant gain in joint space will lead to different effective gains at different configuration in end-effector space, constant gains are directly set in end-effector space instead. As discussed above, we express the error and actuation wrench as 2 dimensional vectors using the bases ξ_i and $\kappa_i\,(i = 1, 2)$. The feedback force F_{fb} that should be applied on the end-effector is computed by:

$$F_{\text{fb}} = K_p e + \int K_i e + K_v \dot{e} \tag{11}$$

where

$$e = (g_d - g)g^{-1} \tag{12}$$

To assign proper gain matrices for (11), note that from (3) and (8) we have:

$$\langle \kappa_1, \xi_1 \rangle = \langle \kappa_2, \xi_2 \rangle = 0, \langle \kappa_1, \xi_2 \rangle = \frac{d}{2}, \langle \kappa_2, \xi_1 \rangle = -\frac{d}{2}. \tag{13}$$

The above equation is clear from the fact that κ_i's are unit pure linear forces and ξ_i's are unit pure rotational velocities (see also Fig. 4). In other words, κ_1 can only suppress pose error along ξ_2 but not ξ_1; κ_2 can only suppress pose error along $\xi_1$but not ξ_2. Therefore, we choose the gain matrices to be of the form:

$$K_p = \begin{bmatrix} 0 & -k_p \\ k_p & 0 \end{bmatrix}, K_i = \begin{bmatrix} 0 & -k_i \\ k_i & 0 \end{bmatrix}, K_v = \begin{bmatrix} 0 & -k_v \\ k_v & 0 \end{bmatrix} \tag{14}$$

Motors are set into torque control mode. Feedback force in end-effector space is pulled back to the actuation torque space $T^*_{f_a(\theta_e)}\Theta_a$:

$$\tau_{a,\text{fb}} = J_I^+ F_{\text{fb}} \tag{15}$$

g is computed by the kinematics based on the information of either two (Fig. 8) or three (Fig. 9) encoders.

C. Antagonistic actuation control

Based on the redundant control scheme above, an amount of constant internal force $F_{\text{int}} \in span\{\kappa_3\}$ is intentionally exerted in order to improve stiffness.

$$\tau_{a,\text{int}} = \hat{J}^T F_{\text{int}} \tag{16}$$

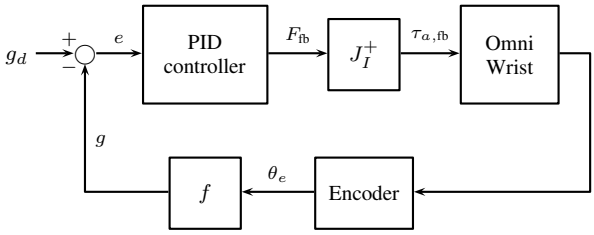

p

Fig. 8. Minimum 2-norm torque control

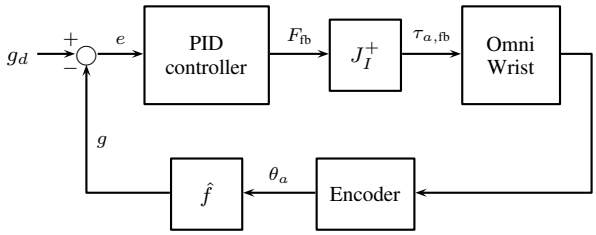

Fig. 9. Minimum 2-norm torque control with redundant encoder

The overall actuation torque is given by:

$$\tau_a = \tau_{a,\text{fb}} + \tau_{a,\text{int}} = J_I^+ F_{\text{fb}} + \hat{J}^T F_{\text{int}} \tag{17}$$

However, it does no harm to replace J_I^+ with $\hat{J}^T$ in the above equation to get a simpler expression for τ_a:

$$\tau_a = \hat{J}^T F, F = F_{\text{fb}} + F_{\text{int}} \tag{18}$$

F cannot be arbitrarily large since τ_a is subject to the following constraints:

$$\tau_a^i = (\hat{J}^T F)^i \in [\tau^i_{a,\min}, \tau^i_{a,\max}], (i = 1, 2, 3) \tag{19}$$

Therefore we propose an antagonistic actuation control scheme with constant internal force, which takes into consideration the joint torque limit (see Fig. 10).

IV. Experiment and Results

A. Experiment Platform

Our experiment platform is shown in Fig. 11. A Precise Automation 2400C series motion controller is used to control *OW*5. To measure the stiffness of this manipulator, we apply static loads to the end-effector via wire and pulley. External wrench can be applied from different directions by varying the location of the pulley on the frame, and is measured by an ATI mini45 force/torque sensor installed on the end-effector. The twist displacement of the end-effector is captured by a camera. Cartesian stiffness matrix is calculated from multiple sets of measurement data using least square method.

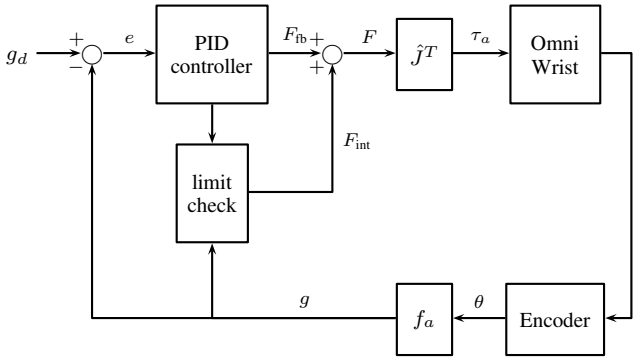

Fig. 10. Antagonistic actuation control scheme with constant internal force

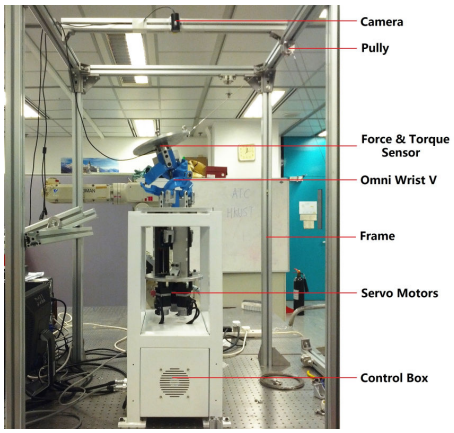

Fig. 11. Experiment platform

TABLE I

STIFFNESS MATRIX $\mathcal{K}_r$ AT $\phi = 70°$, $\psi = 35°$ (UNIT: N/RAD)

Joint space PID	$\begin{bmatrix} 3306 & 1151 \\ -260.4 & 2069 \end{bmatrix}$
Min. 2-norm (model-based)	$\begin{bmatrix} 4439 & -145.3 \\ -117.4 & 2972 \end{bmatrix}$
Min. 2-norm (3-axis)	$\begin{bmatrix} 4857 & 299.3 \\ -178.5 & 4472 \end{bmatrix}$
Constant internal force	$\begin{bmatrix} 7690 & 854.0 \\ 616.6 & 6351 \end{bmatrix}$

B. Result

The stiffness matrix $\mathcal{K}_r$ is measured under different control schemes, all at the configuration $\phi = 70°$ and $\psi = 35°$, and the results are listed in Table I (unit: N/rad). The singular values of $\mathcal{K}_r$ are listed in Table II, which shows an appreciable increase in both the weakest and strongest stiffness under the redundant control schemes. Note that the two singular values of $\mathcal{K}_r$ is also the length of the principal axes of the corresponding force ellipse for unit twist displacements (in the reduced kinetostatics model, there is a well defined metric on both the twist space and the wrench space). The larger the ellipse, the stronger the stiffness. We draw the stiffness ellipse under different control strategies with $\|\Delta g \cdot g^{-1}\| = 0.01$, in which case q is subject to an about $0.5mm$ displacement, as shown in Fig. 12. These ellipses are completely one inside another. The result shows that *OW*5 does have a better stiffness performance under redundant and antagonistic actuation control strategies.

In the case of minimum 2-norm torque control, it is shown that redundant encoder offers a better performance. This is

TABLE II

SINGULAR VALUES OF P$\mathcal{K}_r$ AT $\phi = 70°$, $\psi = 35°$ (UNIT: N/RAD)

Control Scheme	σ_{max}	σ_{min}
Joint space PID	3541	2017
Min. 2-norm (model-based)	4451	2960
Min. 2-norm (3-axis)	4873	4468
Antagonistic stiffness control	8016	6027

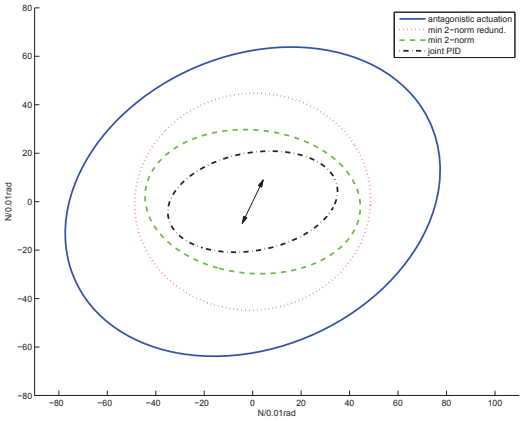

Fig. 12. Stiffness ellipse at $\phi = 70°$, $\psi = 35°$.

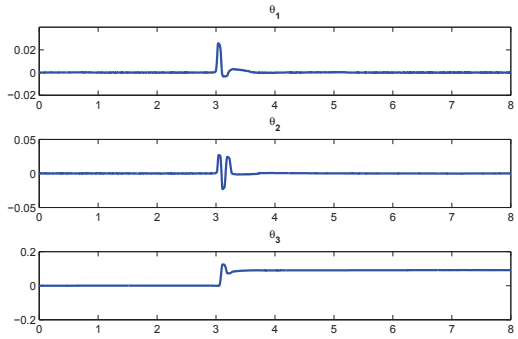

Fig. 13. Encoder reading in model-based mode.

because due to minor joint clearance, θ_3 can still vary while θ_1, θ_2 are fixed. Fig. 13 shows that when a small external disturbance is applied without redundant encoder, θ_3 does not come back to 0 since its error cannot be sensed. If we perturb θ_3 a little bit, q should move along the direction v,

$$v = \hat{J} \cdot (0, 0, 1)^T \tag{20}$$

When redundant encoder is used, the stiffness along v is conceivably improved. This explanation is consistent with the experiment result shown in Fig. 12 (v is indicated by the "$\leftrightarrow$" symbol).

The stiffness matrix $\mathcal{K}_r$ is also measured at several different configurations, and the corresponding ellipses are shown in Fig. 14. Performance under antagonistic control is always the best among the four schemes, which is followed by the minimum 2-norm torque control schemes. At the initial configuration ($\phi = 0°$, $\psi = 0°$), stiffness ellipses of the two minimum 2-norm control schemes overlap each other; the one with redundant encoder still performs better along v.

V. CONCLUSION

In this paper, we present an experimental evaluation of the Cartesian stiffness of *OW*5 under redundant and antagonistic actuation. We first give a brief review of *OW*5's kinetostatics using the mathematical tools of screw theory and homogeneous matrix, which can be summarized into three diagrams (Fig. 2, 3 and 5), and is illustrated in Fig. 4. The Cartesian stiffness is defined to be the linear transformation that prescribes the needed external wrench from the twist displacement of the end-effector. We derive a reduced kine-

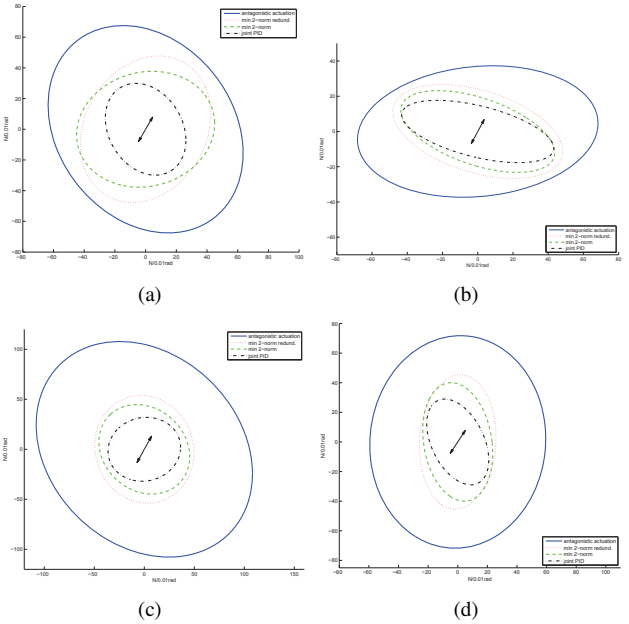

Fig. 14. Stiffness ellipse at (a)$\phi = 0°$, $\psi = 0°$; (b)$\phi = 135°$, $\psi = 40°$; (c)$\phi = 0°$, $\psi = 20°$; (d)$\phi = 250°$, $\psi = 30°$.

tostatics model and stiffness model for *OW*5. The resulting stiffness matrix is 2-by-2 and can be graphically represented as stiffness ellipse. Using the reduced kinetostatics and stiffness model, we formulate four control strategies: joint space PID control, minimum 2-norm torque control without or with redundant encoder, and antagonistic actuation control scheme with constant internal force. The stiffness matrices of *OW*5 are measured under the four control schemes by force/torque sensor and vision. The experiment result under different control schemes are compared and is in favor of the minimum 2-norm control scheme with redundant encoder and the antagonistic control scheme. Both offer an appreciable increase in Cartesian stiffness of *OW*5 in comparison to the joint space PID control scheme.

REFERENCES

[1] T. Brogårdh. Pkm research-important issues, as seen from a product development perspective at abb robotics. In *Workshop on Fundamental Issues and Future Research Directions for Parallel Mechanisms and Manipulators.*, 2002.

[2] M. Morisawa, T. Yakoh, T. Murakami, and K. Ohnishi. A comparison study between parallel and serial linked structures in biped robot system. In *Industrial Electronics Society, 2000. IECON 2000. 26th Annual Confjerence of the IEEE*, volume 4, pages 2614–2619. IEEE, 2000.

[3] M. Weck and D. Staimer. Parallel kinematic machine tools–current state and future potentials. *CIRP Annals-Manufacturing Technology*, 51(2):671–683, 2002.

[4] T. Brogårdh, S. Hanssen, and G. Hovland. Application-oriented development of parallel kinematic manipulators with large workspace. In *Proc. of the 2nd International Colloquium of the Collaborative Research Center*, volume 562, pages 153–170, 2005.

[5] F. Majou, C. Gosselin, P. Wenger, and D. Chablat. Parametric stiffness analysis of the orthoglide. *Mechanism and Machine Theory*, 42(3):296–311, 2007.

[6] J.F. O'Brien and J.T. Wen. Redundant actuation for improving kinematic manipulability. In *Robotics and Automation, 1999. Proceedings. 1999 IEEE International Conference on*, volume 2, pages 1520–1525. IEEE, 1999.

[7] B.J. Yi and R.A. Freeman. Geometric characteristics of antagonistic stiffness in redundantly actuated mechanisms. In *Robotics and Automation, 1993. Proceedings., 1993 IEEE International Conference on*, pages 654–661. IEEE, 1993.

[8] H. Cheng, Y.K. Yiu, and Z.X. Li. Dynamics and control of redundantly actuated parallel manipulators. *Mechatronics, IEEE/ASME Transactions on*, 8(4):483–491, 2003.

[9] L.P. Wang, J. Wu, J.S. Wang, and Z. You. An experimental study of a redundantly actuated parallel manipulator for a 5-dof hybrid machine tool. *Mechatronics, IEEE/ASME Transactions on*, 14(1):72–81, 2009.

[10] D. Chakarov. Study of the antagonistic stiffness of parallel manipulators with actuation redundancy. *Mechanism and machine theory*, 39(6):583–601, 2004.

[11] A. Muller. Stiffness control of redundantly actuated parallel manipulators. In *Robotics and Automation, 2006. ICRA 2006. Proceedings 2006 IEEE International Conference on*, pages 1153–1158. IEEE, 2006.

[12] S. Kock and W. Schumacher. A parallel xy manipulator with actuation redundancy for high-speed and active-stiffness applications. In *Robotics and Automation, 1998. Proceedings. 1998 IEEE International Conference on*, volume 3, pages 2295–2300. IEEE, 1998.

[13] S.B. Nokleby, R. Fisher, R.P. Podhorodeski, and F. Firmani. Force capabilities of redundantly-actuated parallel manipulators. *Mechanism and machine theory*, 40(5):578–599, 2005.

[14] A. Muller. Internal preload control of redundantly actuated parallel manipulators—its application to backlash avoiding control. *Robotics, IEEE Transactions on*, 21(4):668–677, 2005.

[15] M. ValÁšek, V. Bauma, Z. šika, K. Belda, and P. PÍša. Design-by-optimization and control of redundantly actuated parallel kinematics sliding star. *Multibody System Dynamics*, 14(3):251–267, 2005.

[16] Ross-Hime Designs. Omni-wrist v. `http://www.anthrobot.com/omni-wrist-v/`.

[17] W.Q. Wu, Z.X. Li, and J.B. Shi. Geometric properties of zero-torsion parallel kinematics machines. In *Intelligent Robots and Systems (IROS), 2010 IEEE/RSJ International Conference on*, pages 2307–2312. IEEE, 2010.

[18] Y.Q. Wu, I.A. Bonev, G.F. Liu, and Z.X. Li. A study of the double universal joint for high tilt angle parallel wrists. *Journal of Mechanisms and Robotics*, 2012. under revision.

[19] C. Gosselin. Stiffness mapping for parallel manipulators. *Robotics and Automation, IEEE Transactions on*, 6(3):377–382, 1990.

[20] B.S. El-Khasawneh and P.M. Ferreira. Computation of stiffness and stiffness bounds for parallel link manipulators. *International Journal of Machine Tools and Manufacture*, 39(2):321–342, 1999.

[21] S.F. Chen and I.M. Kao. Conservative congruence transformation for joint and cartesian stiffness matrices of robotic hands and fingers. *The International Journal of Robotics Research*, 19(9):835–847, 2000.

[22] N. Ciblak and H. Lipkin. Asymmetric cartesian stiffness for the modeling of compliant robotic systems. In *Proc. 23rd Biennial ASME Mechanisms Conference, Minneapolis, MN*, 1994.

[23] M. Zefran and V. Kumar. Affine connections for the cartesian stiffness matrix. In *Robotics and Automation, 1997. Proceedings., 1997 IEEE International Conference on*, volume 2, pages 1376–1381. IEEE, 1997.

[24] T. Huang, X. Zhao, and D.J. Whitehouse. Stiffness estimation of a tripod-based parallel kinematic machine. *Robotics and Automation, IEEE Transactions on*, 18(1):50–58, 2002.

[25] D. Deblaise, X. Hernot, and P. Maurine. A systematic analytical method for pkm stiffness matrix calculation. In *Robotics and Automation, 2006. ICRA 2006. Proceedings 2006 IEEE International Conference on*, pages 4213–4219. IEEE, 2006.

[26] A. Pashkevich, D. Chablat, and P. Wenger. Stiffness analysis of over-constrained parallel manipulators. *Mechanism and Machine Theory*, 44(5):966–982, 2009.

[27] R.M. Murray, Z.X. Li, and S.S. Sastry. *A mathematical introduction to robotic manipulation*. CRC, 1994.

[28] K.H. Hunt. Constant-velocity shaft couplings: a general theory. *Journal of Engineering for Industry*, 95:455, 1973.

[29] M. Carricato. Decoupled and homokinetic transmission of rotational motion via constant-velocity joints in closed-chain orientational manipulators. *J. Mech. Robot.*, 1(4):1–14, Nov 2009.

[30] L.W. Tsai. *Robot analysis: the mechanics of serial and parallel manipulators*. Wiley-Interscience, 1999.

[31] G.R. Dunlop and T.P. Jones. Position analysis of a 3-dof parallel manipulator. *Mechanism and Machine Theory*, 32(8):903–920, 1997.